Multiple-Antennae Observation and EMTR Processing of Lightning VHF Radiations

TAO WANG, **LI-HUA SHI**, (Member, IEEE), **SHI QIU**, **ZHENG SUN**, **QI ZHANG**, **YAN-TAO DUAN**, AND **BO LIU**

National Key Laboratory on Electromagnetic Environmental Effects and Electro-Optical Engineering, Army Engineering University of PLA, Nanjing 210007, China

Corresponding author: Li-Hua Shi (lihuashi@aliyun.com)

ABSTRACT In order to locate the faint sources in the lightning discharge, an improved broadband VHF observation system is developed. Both the system configuration and locating algorithm are specially designed to locate weak radiation sources from background noise. The proposed system consists of seven broadband omnidirectional antennas in "L" shape and runs in continuous acquisition mode. An electromagnetic time reversal method designed in frequency domain is applied to locate the radiation sources. Two metrics have been introduced to distinguish between actual lightning sources and noise event. Numerical simulations and field calibration are carried out to test the system's performance in locating weak sources. Moreover, the performance on spatial resolution, robustness, and the ability of multi-source localization are investigated. Finally, this system is applied to map the propagation of the upward positive leader (UPL) from a classical triggered lightning with time resolution 0.128 μs. The results prove that the proposed system could well depict the whole progression of UPL until its extinction, and the advantages of the proposed seven antennas array in retrieving weak radiations are presented in detail.

INDEX TERMS VHF, time reversal, lightning location.

I. INTRODUCTION

The VHF time-of-arrival (TOA) [1], [2], short-baseline TDOA [3]–[5] and interferometric techniques [6]–[11] have been widely used to map the detailed development of flashes within storms. For the latter two techniques, usually, three short-baseline antennas are used to determine the direction of lightning VHF radiations by time difference or phase difference estimations, and a sequential record model is often employed. However, few sensors and sequential record model would result in missing some sources at very low received power levels.

In order to locate faint sources, Stock *et al*. [9] developed a continuous broadband digital interferometry (INTF) and four metrics to filter false solutions. Continuous recording has been proved to be more effective than sequentially triggered system in retrieving weak radiations. By virtue of continuous recording technique, Rison *et al*. [6] reveled a fast positive breakdown in narrow bipolar events in nature lightning with the INTF [9]. Stock *et al*. [12] analyzed measurements of fast positive breakdown events in three nature flashes with the same INTF. Zhang *et al*. [13] presented fine structure of the UPL with a flash-continuous broadband interferometer.

Another possible way to improve the location accuracy of faint sources is to make many independent measurements of the emission by deploying additional antennas. A multiple baseline lightning interferometry using four sensors is proposed in [14] and [15]. However, "for faint sources, the least squares regression technique used in [14] is very prone to locating a side lobe of the cross correlation, instead of the correct maximum," and the probability of the error occurring with more antennas being used.

Recently, EMTR technique [18] has been successfully used in lightning localization, which can automatically converge the energy of the TR signals to the source direction and is applicable to arbitrary array. In addition, unlike the TOA techniques and interferometric techniques, EMTR method needs not to estimate the time or phase difference and is capable of recognizing multiple sources in the same time window. Lugrin *et al*. [16] and Mora *et al*. [17] applied EMTR technique to locate the lightning striking point. Wang *et al*. [18] used this method with four antennas to locate multiple sources and the sources on the low elevation, which proved that EMTR technique performed better than traditional interferometric method [15], [19].

This paper operates the EMTR-VHF method of [18] with multiple-antennae array to reproduce the lightning processes, especially the weak radiation regions. The array consists of seven VHF antennas in an "L" shape configuration. The paper is organized as follows. In Section II the basic principles of EMTR-VHF method designed in frequency domain (FD) are illustrated, and two metrics are proposed to distinguish between actual lightning sources and noise events. Section III presents the simulated results of EMTR-VHF method operating with the L array, and some comparisons versus the three-element array are taken. In Section IV, field experiments on locating the artificial radiation sources are carried out. In Section V, the localization results of a triggered lighting are presented and analyzed. The last section is conclusions and discussions.

II. EMTR-VHF METHOD

In this section, EMTR-VHF method operating on an arbitrary planar array is derived in the form of frequency domain. Different from the EMTR-VHF method in time domain in [18], operating the method in FD avoids the influence of sample interval on the localization accuracy of the algorithm. In addition, if there are some interference bands in the signal, it is convenient to remove them directly for the FD algorithm.

At last, two metrics to filter false solutions are defined.

A. EMTR-VHF METHOD

Suppose that an planar array in free space consists of M elements with known positions $A_m = (x_m, y_m)$, $m = 1, 2, 3, \cdots, M$; a distant broadband VHF signal $s(t)$ arrives at the array from the direction $\varpi_s = (\varphi_s, \theta_s)$ relative to the origin of the coordinate system, where θ is the elevation and φ is the azimuth. Then, the receiving signals $u_m(t)$ at each elements can be expressed as

$$u_m(t) = s(t + \tau_m) + n_m(t) \tag{1a}$$

$$\tau_m(\varpi_s) = -(x_m \cos\theta_s \cos\varphi_s + y_m \cos\theta_s \sin\varphi_s)/c \tag{1b}$$

where τ_m represents the time delay between the mth sensor and the original point; c is the light velocity in free space; $n_m(t)$ represents the noise.

The DFT of (1a) can be expressed in matrix form:

$$U(f_k)$$
$$= a(f_k, \varpi_s) S(f_k) + N(f_k) \tag{2a}$$
$$a(f_k, \varpi_s)$$
$$= \begin{bmatrix} \exp(j2\pi f_k \tau_1) \\ \cdots \\ \exp(j2\pi f_k \tau_m) \end{bmatrix}$$
$$= \begin{bmatrix} \exp\left(-j2\pi f_k \dfrac{x_1 \cos\theta_s \cos\varphi_s + y_1 \cos\theta_s \sin\varphi_s}{c}\right) \\ \vdots \\ \exp\left(-j2\pi f_k \dfrac{x_m \cos\theta_s \cos\varphi_s + y_m \cos\theta_s \sin\varphi_s}{c}\right) \end{bmatrix} \tag{2b}$$

where "T" denotes transpose; f_k represents the kth sampled frequency point, $k = 1, 2, 3, \cdots, K$; $U(f_k) = [U_1(f_k), \cdots, U_M(f_k)]^T$ represents the received M complex vector in FD at each frequency point; $a(f_k, \varpi_s)$ is a delay vector including the delay coefficient of each sensor at f_k; $N(f_k) = [N_1(f_k), \cdots, N_M(f_k)]^T$ is the noise vector.

Conjugate $U(f_k)$ and retransmit it to the space. The conjugate operation here is equivalent to time reverse the signals in time domain. Then a synthesized signal in FD is obtained in the ith direction ϖ_i. And ϖ_i is determined by meshing the $\varphi\theta$-plane into N directions, $i = 1, 2, 3, \cdots, N$. The synthesized signal can be expressed as

$$
\begin{aligned}
Y(f_k, \varpi_i) &= U^H(f_k) a(f_k, \varpi_i) \\
&= S^H(f_k) a^H(f_k, \varpi_s) a(f_k, \varpi_i) + N^H(f_k) a(f_k, \varpi_i) \\
&= S^H(f_k) a^H(f_k, \varpi_s) a(f_k, \varpi_i) \\
&\quad + \sum_{m=1}^{M} N_m(f_k) \exp(j2\pi f_k \tau_m)
\end{aligned} \tag{3}
$$

where "H" denotes complex conjugate transpose; $Y(f_k, \varpi_i)$ represents the FD synthesized signal in the ith direction. As the second item on the right of (3) shows, multiple superposition will reduce noise due to its randomness. Therefore, the performance of the algorithm is improved by using multiple-antennae array.

From equation (2) and (3), it is only in the original source direction where the retransmitting signals add in phase. And the energy of the synthesized signal in the ith direction can be calculated by

$$P(\varpi_i) = \sum_{k=1}^{K} |Y(f_k, \varpi_i)|^2 \tag{4}$$

Then, we can estimate the source direction by searching the peak position of the following function on the $\varphi\theta$-plane.

$$\varpi_s = \arg\{\max[P(\varpi_i)]\} \tag{5}$$

According to the above derivations, estimating the ϖ_s with EMTR-VHF method allows the principal components to add in phase and be reinforced, while makes the random components add randomly and tend to be "counteracted". It means that this method is capable of extracting the signal components from the receiving array data and suppressing the noise components. Obviously, with more receivers contributing to the coherent superposition the principal components will be further strengthened, which coincides with our aim to locating the faint radiations.

B. IMPLEMENTATION

The broadband VHF radiations are recorded with 12-bit resolution at a sampling rate of 500MHz continuously for 500ms with 250ms pretrigger time by an eight-channel LeCroy digital storage oscilloscope (DSO). The recorded signals were postprocessed utilizing the proposed method and applied to successive of overlapping data windows from the time series waveforms. For the triggered lighting recorded in this study,
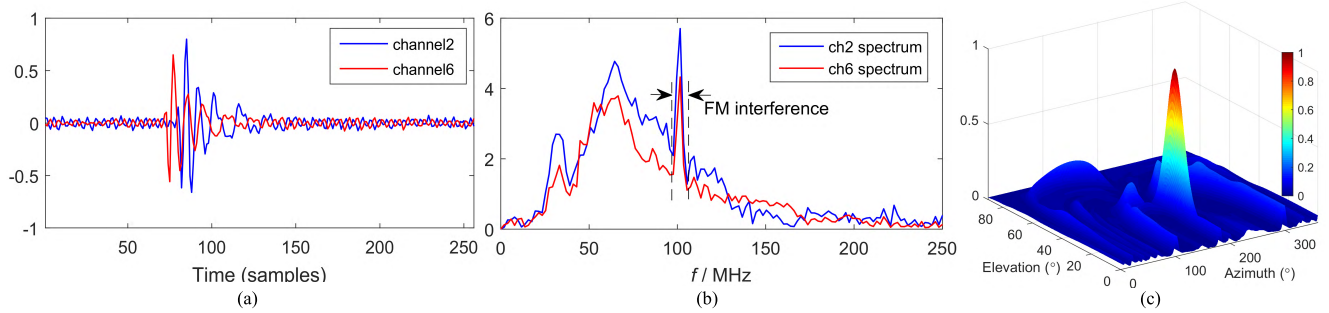
FIGURE 1. A temporally isolated radiation event of the triggered lightning of section V, illustrating the processing technique used to determine $P(\varpi_i)$ distributing on the $\varphi\theta$-plane. (a) Normalized waveforms from the two channels for a 256 (512 ns) sample window; (b) spectrum of the two signals; (c) distribution of normalized $P(\varpi_i)$ for this isolated radiation event by the EMTR-VHF method.

the data segments are 256 samples (512ns) in length, and successive windows are displaced 64 samples (128ns) relative to the preceding window.

For a single window including an impulsive radiation event of the triggered lighting, the process of determining $P(\varpi_i)$ distribution on the $\varphi\theta$-plane is depicted in Fig. 1.

Fig. 1(a) shows two channel waveforms within a 256 sample window, with the vertical scale representing normalized amplitude. It is apparent that channel 6 (red) is advanced relative to channel 2 (blue).

Fig. 1(b) shows the frequency spectrum of the two signals. In this figure, the narrow band FM interference around 100 MHz is intensive.

In this study, we directly remove the FM frequency components during postprocessing. Finally, the frequency range 25MHz $\sim$ 90MHz and 110MHz $\sim$ 150MHz is selected for the localization algorithm.

Fig. 1(c) shows the energy $P(\varpi_i)$ distribution on the $\varphi\theta$-plane which is meshed with grid size 0.1° × 0.1°. Through searching the location of the $P(\varpi_i)$ peak in the plane, the direction to the impulsive radiation event will be obtained. Actually, scanning with smaller grid length will be computationally intensive. In this paper, two step spatial searching method is proposed: (1) a large grid length, 1° in this paper, is employed to get a rough position as a predictive solution on the $\varphi\theta$-plane; (2) a fine grid length 0.01° is utilized to obtain a precise orientation in a small area which centers on the predictive solution and expands outward a few degrees, 1.5° used in this paper. The two step spatial searching method performs well in enhancing both computational efficiency and angular resolution without searching the whole space with fine precision.

C. NOISE REDUCTION

Continuous recording and a heavy overlap (75% in this paper) used in the process of implementation can produce numerous solutions of which a considerable amount are either contaminated by or entirely produced by noise. The noise solutions would significantly degrade the lightning mapping quality.

A robust noise reduction technique is therefore critical to the full utilization of the data. Here, two metrics are

developed to distinguish between actual lightning sources and noise events.

One of the two metrics is named as coherence ratio (CR) which is made possible by the overlap analysis procedure and provides a distribution of solutions within a few successive overlapping windows.

Due to the heavy overlap, the windows are not all independent, and so the sources appears to slowly drift over a small region during a short duration in the sky. For the wth time window, we can obtain a corresponding solution ϖ_w, $w = 1, 2, 3, \cdots, W$. Then, centering on this time window, $Q/2$ solutions ϖ_q ($q = 1, 2, 3, \cdots, Q$) on its right and left sides are selected respectively. The sphere distance D between ϖ_w and ϖ_q can be obtained. Considering a short duration, Q should not be set to a large value. Finally, CR is defined as the number of ϖ_q with $D < \Delta\phi$ divided by Q.

$$D = \|\varpi_w - \varpi_q\| \tag{6a}$$

$$CR = \frac{Q(D < \Delta\phi)}{Q} \tag{6b}$$

where $\Delta\phi$ is an acceptable distance threshold and determined by subjectively evaluating the results. $Q(D < \Delta\phi)$ represents the number of ϖ_q with $D < \Delta\phi$. Solutions due to noise alone tend to shift large distances across the sky. Locations having small values of CR are likely to seriously deviate from the distribution of solutions within Q successive overlapping windows and are eliminated for further consideration.

The second metric is named as energy ratio (ER) which is defined to evaluate the concentration of $P(\varpi_i)$ mapping on the $\varphi\theta$-plane and can be calculated by equation (7).

$$ER = \ln\left(\frac{\max[P(\varpi_i)]}{\frac{1}{N}\sum_{i=1}^{N} P(\varpi_i)}\right) \tag{7}$$

The ER metric defines the concentration from the perspective of the energy of the synthesized signal. In this case, sources having low values of ER metric are likely to be in error and will be eliminated.
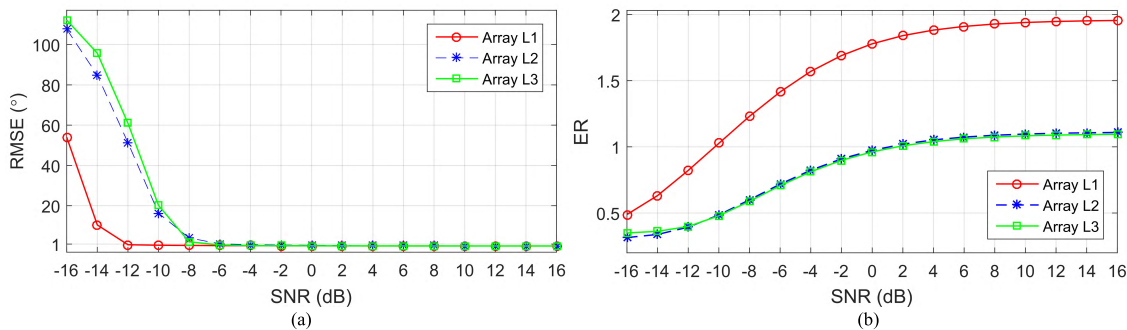
FIGURE 2. Simulation results for array L1, L2 and L3: (a) RMSE versus SNR; (b) ER versus SNR.

III. NUMERICAL SIMULATIONS

In this section, numerical simulations are conducted to investigate the influence of the number of antennas on the localization of the radiation source, including localization accuracy, spatial resolution, and robustness.

The array used in this section consists of seven elements in an "L" shape configuration which is the same with the one employed in field measurement, as shown in Fig. 4. The waveform of the radiation source is assumed to be a Gaussian pulse modulated oscillation in the form of (8)

$$s(t) = A_0 \sin(2\pi f_0 t) \, e^{-4\pi\left(\frac{t-\tau_1}{\tau_2}\right)^2} \tag{8}$$

where f_0 is the center frequency; τ_1 and τ_2 are the parameters that regulates the bandwidth of the signal; A_0 the amplitude of the signal.

During the simulation, we set f_0 = 100 MHz, $\tau_1 = \tau_2 = 30$ ns, and the frequency range is $0 \sim 200$MHz. The noise is assumed to be the Gaussian noise with zero mean and variance σ^2.

In order to study the influence of the number of antennas on the EMTR-VHF method, especially its performance for faint sources localization, we respectively select three kinds of combinations from the L array in Fig. 4: (1) seven elements, including $V_1, V_2, \cdots, V_7$, represented as L1; (2) three elements, including V_3, V_4, V_5, represented as L2; (3) three elements, including V_1, V_4, V_7, represented as L3. The baselines of L2 and L3 are 9m and 27m, respectively.

A. ROBUSTNESS

Assuming a plane wave incident from $\varpi_s = (120°, 30°)$, the received signals acquired by three antennas in the array can be derived using equation (1), meanwhile white Gaussian noise with different SNR levels are added independently to each channel. The results shown in Fig. 2(a) are derived from 10000 independent trials, with the RMSE computed from

$$\text{RMSE} = \sqrt{\frac{1}{10000} \sum_{n=1}^{10000} \|\varpi_n - \varpi_s\|^2} \tag{9}$$

where ϖ_n is the nth DOA estimation at each SNR level.

Fig. 2(a) shows that increasing number of sensors improves the anti-interference ability of localization algorithm. The RMSE value is less than 1° for array L1 case even when SNR is greater than -12dB, which means quite a low noise level. In contrast, the corresponding noise level for the array L2/L3 case is -6dB. Besides, with 10000 times addition of random noises for each SNR level, we can obtain corresponding ER every time. Fig. 2(b) shows the statistical mean results of ER versus SNR.

As shown in Fig. 2(b), ER for array L1 case is greater than array L2/L3 cases, which means the array L1 owns higher concentration of $P(\varpi_i)$ mapping on the $\varphi\theta$-plane and is helpful to retrieve weak source.

Therefore, the array L1 consisting of seven sensors performs better in locating weak sources than the array L2/L3.

B. SPATIAL RESOLUTION

In order to compare the spatial resolution of array L1, L2 and L3, the simulation is carried out for the three combinations with SNR = 10dB, respectively. Localization results for the three cases are shown in Fig. 3(a-c) respectively. For a given angle (120°, 30°), the cures of the normalized energy versus azimuth/elevation are plotted in Fig. 3(d), where half peak width of the main lobe is defined as the spatial resolution of azimuth and elevation, noted by SRA and SRE respectively.

As Fig. 3(a-c) shows, array L1 performs better in mapping $P(\varpi_i)$ on the $\varphi\theta$-plane with lower side lobes which are less than 20% of the main lobe, and the side lobes of array L2/L3 reach 60% of their main lobes. The presence of high side lobes can cause misjudgment of the radiation sources, especially for the faint sources.

As shown in Fig. 3(d), spatial resolutions of the three arrays are different. It illustrates that longer baseline provides better spatial resolution. But it is noteworthy that the number and intensity of the secondary peaks increase obviously for the results of array L2 and L3 in Fig. 3(b-c). Finally, the conclusion can be drawn that the increase of the element number can enhance the directivity of the array and suppress the side lobes at the same time.
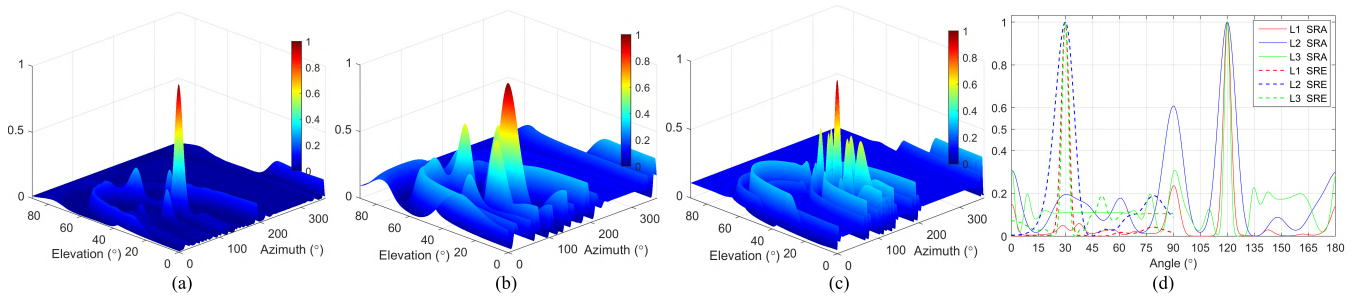
FIGURE 3. Spatial resolution comparison results: (a-c) simulation results by L1, L2 and L3 respectively; (d) SRA and SRE for the three arrays.
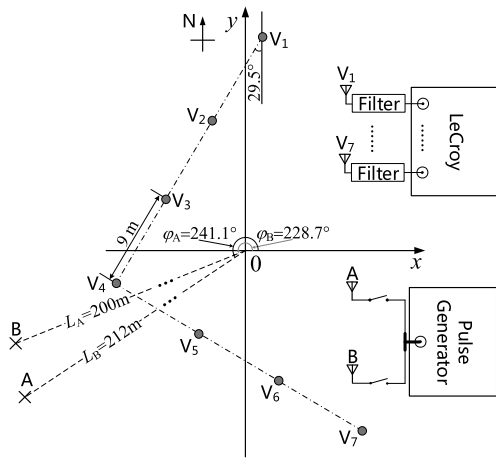

FIGURE 4. Schematic diagram of experimental setup.

IV. EXPERIMENTAL VALIDATION

Field experiments are carried out to test the proposed method with the "L" array mentioned earlier. Seven VHF broadband omnidirectional antennas are arranged with baseline of 9m. Broadband VHF radiations are digitized at a rate of 1.25GHz with 12-bit resolution by an eight channel LeCroy DSO. The system configuration diagram is shown in Fig. 4, which is also utilized in Section III and Section V.

A. SINGLE WEAK RADIATION SOURCE CASE

Here, we focus on testing the performance of the array on locating the weak radiation source. In the test, we set the excitation source at low power level. The signal from A acquired by the array is shown in Fig. 5(a), where the actual signals are marked by the double-head pink rows.

As Fig. 5(a) shows, the SNR of the array recording signals is quite low. For the seven channels, the SNR estimations are 2.6dB, 1.7dB, 0.4dB, −0.4dB, −4.3dB, −0.6dB, and 0.1dB respectively. The results and their corresponding errors are shown in Fig. 5(b-d), which indicate that the $P(\varpi_i)$ mapping quality by array L1 is the best among the three arrays and its error is the smallest. The error here is the difference between estimated angle and true value. The results by the other two subarrays show that the sidelobes ring heavily and almost submerge the main lobe. The test results show that the array

with seven elements performs better in locating the weak radiation source than the three elements array.

B. LOCALIZATION FOR MULTIPLE EMITTERS

In this section, A and B are synchronously excited to test the capability of the proposed method in retrieving multiple emitters.

As shown in Fig. 6(a), it is easy to divide the acquiring waveforms into two signals. But for the more general cases, if the positions of the two sources are unknown, it is difficult to match the receiving signal with the two emitters. The algorithms based on estimating the time or phase difference will fail to locate the sources with the acquiring data. In this paper, EMTR-VHF method without time delay estimation is applied to the multi-sources data. The results obtained by the proposed method with array L1 is shown in Fig. 6(b), which illustrates the proposed algorithm performs well in resolving multiple sources. However, as shown in Fig. 6(c-d), the results by array L2 and L3 with three elements present poor mapping quality and large error, even for array L3 with the longest baseline. Comparisons of the results for multiple emitters shows that more elements for an array provides stronger ability in multi-sources localization.

V. TRIGGERED LIGHTNING OBSERVATIONS AND RESULTS

During the summer of 2017, a lightning observation and artificial lightning triggering experiment is conducted in Jiangsu province, China. 23:10:42 on 1 August, a negative lightning is triggered by classical artificial trigger technique in the absence of subsequence return stroke, called as slow discharges [20]. An UPL initiates from the rocket to propagate upward into the cloud and produces an initial continuous current (ICC) that lasts to the end. Triggered lightning provides a good case to verify performances of the algorithm for the faint nature of UPL emissions.

The discharge that we analyze was triggered at 23:10:42 by a rocket trailing a steel wire. The "L" array observation system working in continuous recording model, shown in Fig. 4, was installed at a site 1.1km distant from the rocket launcher, with 188.35° azimuth relative to the observation site.
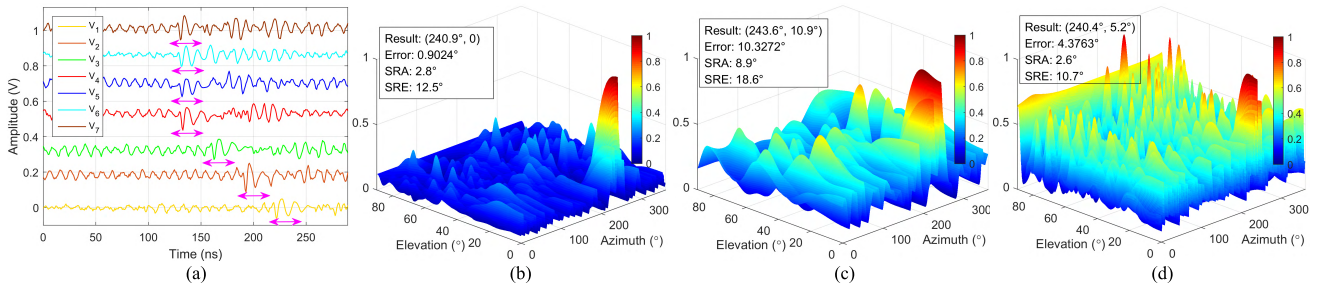
FIGURE 5. Experimental results for single emitter A: (a) array recording signals; (b) result by L1; (c) result by L2; (d) result by L3.
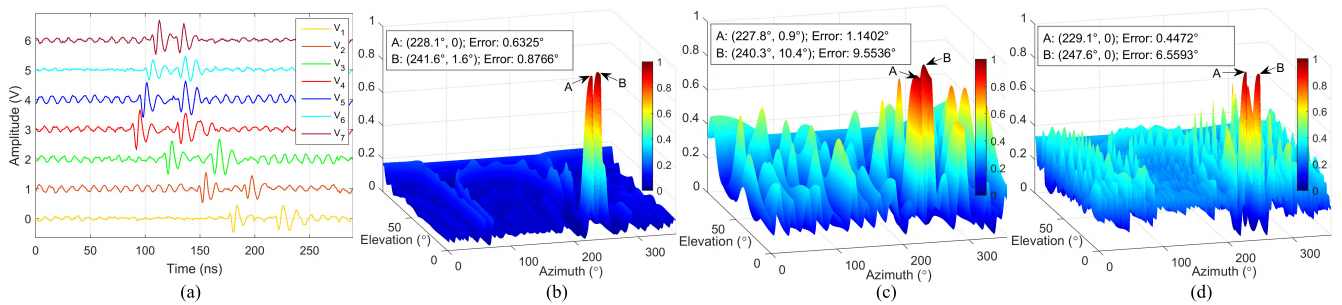

FIGURE 6. Experimental results for multiple emitters, A and B: (a) signals recorded by the array; (b) result by L1; (c) result by L2; (d) result by L3.
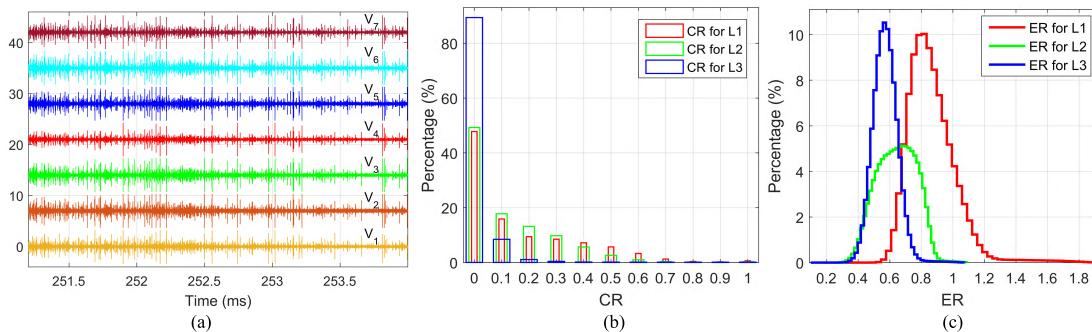

FIGURE 7. Data and CR, ER results for L1, L2 and L3: (a) waveforms recorded by the VHF array; (b) CR results; (c) ER results.

A section (251-254ms) of the time series waveforms received by different antennas are shown in Fig. 7(a), which contains both faint and strong emissions. The entire waveform for the triggered lightning in this study lasts 500ms. The processing provides elevation and azimuth angles of the VHF sources with $0.128\mu s$ time resolution, and it produces 3905426 solutions. During the processing, different results by the array L1, L2, and L3 are obtained respectively. Meanwhile, the two metrics, CR and ER defined in Section II Part C, are also calculated to distinguish the actual and noise solutions.

For the definition of CR in equation (6), $Q = 10$ and $\Delta\phi = 3°$ are selected in this paper. According to the length of the window (512ns) and overlap (128ns), a given time-isolated event would be detected in as many as $512/128 = 4$ overlapping windows, which implies that at least three solutions contribute to this event. Here, the threshold we set for

CR is 0.3, and solutions with CR $\leq$ 0.3 will be filtered. The statistical results of CR are shown in Fig. 7(b). For array L1, L2 and L3, the number of solutions with CR $\geq$ 0.3 take up 26.99%, 19.83% and 1.14% of the number of initial solutions respectively. Obviously, array L1 with seven elements produces the most solutions passing the CR threshold.

A plot of the statistical results of ER for array L1, L2 and L3 is presented in Fig. 7(c). This metric is used to further eliminate the noise solutions. The threshold for ER can be determined by subjectively evaluating the results.

A. FILTERING OF FALSE SOLUTIONS
The filtering of false solutions using metrics is done in two phases. Take the results by array L1 for example, Fig. 8(a) shows all the solutions in the entire sky before removing any noise solutions, the progresses of filtering false solutions are depicted as follows. Note that the map of the triggered
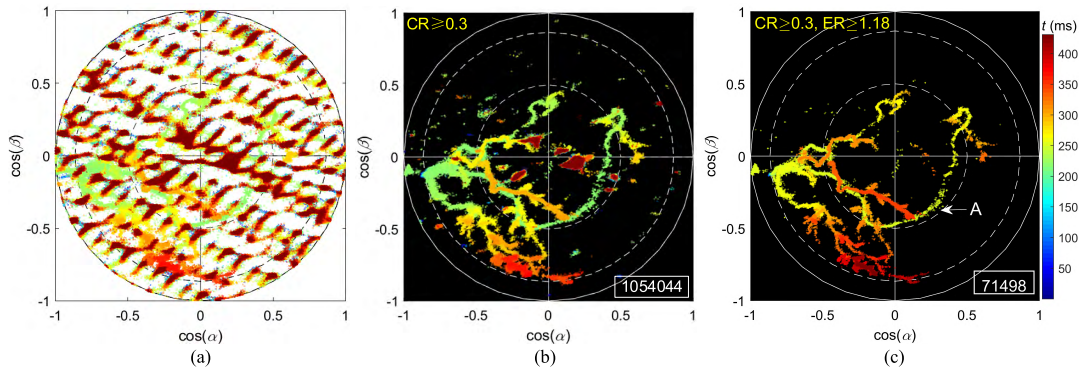
FIGURE 8. Phases of noise reduction for the results by array L1: (a) raw array data prior to any metric filtering; (b) phase 1 noise reduction; (c) phase 2 noise reduction.
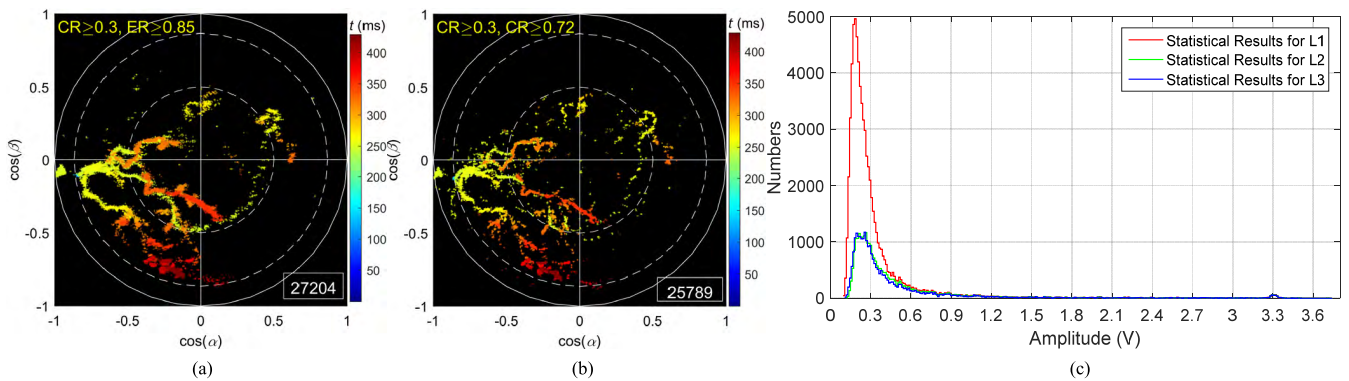
FIGURE 9. Mapping results by array L2 and L3: (a) results by L2; (b) results by L3; (c) statistical results of the receiving signal amplitude for results by L1, L2 and L3.

lightning is shown in the direction cosine planar projection using $\cos\alpha = \cos\theta\cos\varphi$, $\cos\beta = \cos\theta\sin\varphi$, similarly hereinafter.

1) Phase 1

In this phase, the first metric CR is used to filter the false solutions which scatters irregularly in the sky. Those false solutions are inferred to be either contaminated by or entirely produced by noise. Fig. 8(b) shows the results for array L1 after the first phase. The number of remaining solutions is shown in the rectangular box.

2) Phase 2

In this phase, the metric ER is used to further filter the remaining noise solutions after phase 1. For ER is related signal intensity to some extent, some important low power sources might also be removed if its threshold is set too large. In this paper, the threshold ER = 1.18 is selected for the results by array L1 to heavily filter false solutions and obtain a better mapping results. The final version for the results is shown in Fig. 8(c), in which ∼2% of the raw solutions remains and almost no noise sources are left.

As shown in Fig. 8(c), the flash was initiated 244ms later at 30.11° elevation and 188.2° azimuth (red triangle). The azimuth estimation for the flash origin is consistent with the orientation of the rocket launcher (188.35°).

Immediately following initiation, UPL developed upward. Subsequently, copious positive breakdown events was detected developing away from the flash origin in multiple directions from 245ms to 430ms.

B. COMPARISONS OF RESULTS BY ARRAY L1, L2 AND L3

In order to illustrate the impact of the element number on localization, the two phases to filter false solutions are also implemented to the results by array L2 and L3. The two metrics set for the two results are CR $\geq$ 0.3 and ER $\geq$ 0.85 for array L2, and CR $\geq$ 0.3 and ER $\geq$ 0.72 for array L3. The final versions of the results are shown in Fig. 9(a) and (b), respectively.

Comparing the results in Fig. 8(c), Fig. 9(a) and Fig. 9(b), it illustrates that: (i) the locatable VHF sources for the triggered lightning by array L1 is the most among the three results; (ii) the details of the development of UPLs in this lightning are well mapped by array L1, but some of the discharge branches are not mapped clearly by array L2 and L3, especially the longest branch A almost cannot be located by array L3; (iii) some branches present high spatial resolution in L3 results but poor in L2 results, however, L1 results provide high robustness for the entire flash. Actually the phenomenon in (iii) is consistent with the simulation results in Fig. 3, which proves that array with long baseline can provide high spatial

resolution, but few elements makes it more susceptible to the environment noise.

For further comparisons of performances of the three arrays in locating weak sources, Fig. 9(c) shows the statistical results of the receiving signal amplitude for each overlapping window corresponding to solutions of final versions of the three results. Obviously, the number of faint sources located by array L1 is the most among the three arrays, which verifies the significant advantages of array with multiple elements in locating weak emissions.

VI. SUMMARY AND DISCUSSION

In this paper, a multiple-antennae observation system is developed to locate the faint sources in the lightning discharge, especially during the UPLs. Seven broadband omnidirectional antennas are configured in "L" shape for the proposed system using continuous recording mode. A LeCroy DSO is used to acquire signals in seven channels at sampling rate of 500MHz, and the lightning VHF radiations can be recorded for 500ms. EMTR method derived in frequency domain is designed for this system to locate weak emissions. Two metrics are developed to distinguish between actual lightning sources and noise events, based on which the false solutions are filtered effectively.

In order to validate the performances of the proposed system in locating faint sources, some simulations and experimental researches are carried out. The statistical simulation results under various conditions are given, which show the improvement in robustness and resolution as well as the high performance in precision by employing the multi-antennae array. In experimental section, the validity of the proposed system in locating weak sources and multi-sources is tested and verified in practical situations.

Finally, the proposed system is applied to map the propagation of the UPL from a classical triggered lightning. The results presented that the proposed system could map the whole progression in greater details by using array with seven elements than three-element array. And the results also proves that much more copious weaker VHF radiations could be located by the seven-element array than by the three-element array.

It is well known that localizations of the lowest amplitude sources are of particular important for they may show the development of physical processes which were difficult measure in the past, especially for the weak positive leaders. And the multi-elements observation system could be considered as a good tool to complete this work.

REFERENCES

[1] H. E. Edens *et al.*, "VHF lightning mapping observations of a triggered lightning flash," *Geophys. Res. Lett.*, vol. 39, no. 19, p. L19807, 2012, doi: 10.1029/2012GL053666.

[2] J. R. Thomas *et al.*, "Accuracy of the lightning mapping array," *J. Geophys. Res.*, vol. 109, no. D14, p. D14207, 2004, doi: 10.1029/2004JD004549.

[3] Z. Sun, X. Qie, M. Liu, D. Cao, and D. Wang, "Lightning VHF radiation location system based on short-baseline TDOA technique—Validation in rocket-triggered lightning," *Atmos. Res.*, vols. 129–130, pp. 58–66, Jul. 2013.

[4] Z. Sun, X. Qie, M. Liu, R. Jiang, Z. Wang, and H. Zhang, "Characteristics of a negative lightning with multiple-ground terminations observed by a VHF lightning location system," *J. Geophys. Res. Atmos.*, vol. 121, no. 1, pp. 413–426, 2016.

[5] Z. Sun *et al.*, "Characteristics of a rocket-triggered lightning flash with large stroke number and the associated leader propagation," *J. Geophys. Res.*, vol. 119, no. 23, pp. 13388–13399, 2014, doi: 10.1002/2014JD022100.

[6] W. Rison *et al.*, "Observations of narrow bipolar events reveal how lightning is initiated in thunderstorms," *Nature Commun.*, vol. 7, Feb. 2016, Art. no. 10721, doi: 10.1038/ncomms10721.

[7] X. M. Shao, D. N. Holden, and C. T. Rhodes, "Broad band radio interferometry for lightning observations," *Geophys. Res. Lett.*, vol. 23, no. 15, pp. 1917–1920, 1996.

[8] S. Qiu, B.-H. Zhou, L.-H. Shi, W.-S. Dong, Y.-J. Zhang, and T.-C. Gao, "An improved method for broadband interferometric lightning location using wavelet transforms," *J. Geophys. Res.*, vol. 114, no. D18, p. D18211, 2009, doi: 10.1029/2008JD011655.

[9] M. G. Stock *et al.*, "Continuous broadband digital interferometry of lightning using a generalized cross-correlation algorithm," *J. Geophys. Res. Atmos.*, vol. 119, no. 6, pp. 3134–3165, 2014.

[10] S. Yoshida *et al.*, "Three-dimensional imaging of upward positive leaders in triggered lightning using VHF broadband digital interferometers," *Geophys. Res. Lett.*, vol. 37, no. 5, p. L05805, 2010, doi: 10.1029/2009GL042065.

[11] S. Yoshida *et al.*, "The initial stage processes of rocket-and-wire triggered lightning as observed by VHF interferometry," *J. Geophys. Res. Atmos.*, vol. 117, no. D9, p. D09119, 2012, doi: 10.1029/2012JD017657.

[12] M. G. Stock, P. R. Krehbiel, J. Lapierre, T. Wu, M. A. Stanley, and H. E. Edens, "Fast positive breakdown in lightning," *J. Geophys. Res. Atmos.*, vol. 122, no. 15, pp. 8135–8152, 2017, doi: 10.1002/2016JD025909.

[13] Y. Zhang *et al.*, "Observations of the initial stage of a rocket-and-wire-triggered lightning discharge," *Geophys. Res. Lett.*, vol. 44, no. 9, pp. 4332–4340, 2017, doi: 10.1002/2017GL072843.

[14] M. G. Stock and P. R. Krehbiel, "Multiple baseline lightning interferometry—Improving the detection of low amplitude VHF sources," in *Proc. Int. Conf. Lightning Protection (ICLP)*, Shanghai, China, Oct. 2014, pp. 293–300.

[15] M. G. Stock, "Broadband Interferometry of lightning," Ph.D. dissertation, Sci. Phys., Langmuir Lab., New Mexico Inst. Mining Technol., Socorro, NM, USA, 2014.

[16] G. Lugrin, N. M. Parra, F. Rachidi, M. Rubinstein, and G. Diendorfer, "On the location of lightning discharges using time reversal of electromagnetic fields," *IEEE Trans. Electromagn. Compat.*, vol. 56, no. 1, pp. 149–158, Feb. 2014.

[17] N. Mora, F. Rachidi, and M. Rubinstein, "Application of the time reversal of electromagnetic fields to locate lightning discharges," *Atmos. Res.*, vol. 117, pp. 78–85, Nov. 2012.

[18] T. Wang, S. Qiu, L.-H. Shi, and Y. Li, "Broadband VHF localization of lightning radiation sources by EMTR," *IEEE Trans. Electromagn. Compat.*, vol. 59, no. 6, pp. 1949–1957, Dec. 2017.

[19] R. Mardiana and Z.-I. Kawasaki, "Dependency of VHF broad band lightning source mapping on Fourier spectra," *Geophys. Res. Lett.*, vol. 27, no. 18, pp. 2917–2920, 2000.

[20] P. Hubert and P. Laroche, "Triggered lightning in New Mexico," *J. Geophys. Res.*, vol. 89, no. D2, pp. 2511–2521, 1984.

TAO WANG was born in Henan, China, in 1988. He received the B.S. degree from Zhengzhou University, Henan, China, in 2011, and the M.S. degree from the PLA University of Science and Technology, Nanjing, China, in 2014, where he is currently pursuing the Ph.D. degree. His research interests include lightning detection, protection, and electromagnetic compatibility.

LI-HUA SHI (M'96) was born in Hebei, China, in 1969. He received the B.S. degree from Xidian University, Xian, China, in 1990, and the Ph.D. degree from the Nanjing University of Aeronautics and Astronautics, Nanjing, China, in 1996. He is currently a Professor and the Director of the National Key Laboratory on Electromagnetic Environmental Effects and Electro-Optical Engineering, Army Engineering University of PLA, Nanjing, China, with a focus on time-domain measurement and signal processing technology. He is a member of the IEEE EMC Society and an HEMP Fellow of the Summa Foundation, USA.

SHI QIU was born in Shandong, China, in 1984. He received the B.Sc. and Ph.D. degrees from the PLA University of Science and Technology, Nanjing, China, in 2005 and 2012, respectively. He is currently an Associated Professor with the National Key Laboratory on Electromagnetic Environmental Effects and Electro-Optical Engineering, Army Engineering University of PLA. His research interests include lightning physics and lightning protection.

ZHENG SUN was born in Henan, China, in 1987. He received the B.E. degree from Southeast University, Nanjing, China, in 2009, and the Ph.D. degree from the PLA University of Science and Technology, Nanjing, in 2014. He is currently a Lecturer with the National Key Laboratory on Electromagnetic Environmental Effects and Electro-Optical Engineering, Army Engineering University of PLA, Nanjing. His research interests include lightning protection and computational electromagnetics.

QI ZHANG was born in Shandong, China, in 1987. He received the B.E. degree from Guangxi University, Nanning, in 2009, and the M.S. and Ph.D. degrees from the PLA University of Science and Technology, Nanjing, China, in 2012 and 2015, respectively. He is currently a Lecturer with the National Key Laboratory on Electromagnetic Environmental Effects and Electro-Optical Engineering, Army Engineering University of PLA, Nanjing, China. His research interests include lightning protection and computational electromagnetics.

YAN-TAO DUAN was born in Hebei, China, in 1980. He received the B.S., M.S., and Ph.D. degrees in electric systems and automation from the Nanjing Engineering Institute, Nanjing, China, in 2002, 2006, and 2010, respectively. He is currently a Lecturer with the National Key Laboratory on Electromagnetic Environmental Effects and Electro-optical Engineering, Army Engineering University of PLA, Nanjing, China. His research interests include computational electromagnetics and EMP.
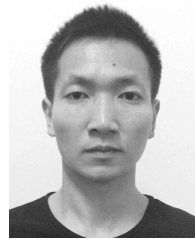
BO LIU was born in Hunan, China, in 1991. He received the B.E. and M.S. degrees from the PLA University of Science and Technology, Nanjing, China, in 2013 and 2016, respectively. He is currently pursuing the Ph.D. degree with the Army Engineering University of PLA. His research interests include lightning detection, protection, and electromagnetic compatibility.

• • •